

Visual Explanation for Identification of the Brain Bases for Dyslexia on fMRI Data

Laura Tomaz Da Silva · Nathalia Bianchini
Esper · Duncan D. Ruiz · Felipe
Meneguzzi · Augusto Buchweitz

Received: date / Accepted: date

Abstract Brain imaging of mental health, neurodevelopmental and learning disorders has coupled with machine learning to identify patients based only on their brain activation, and ultimately identify features that generalize from smaller samples of data to larger ones. However, the success of machine learning classification algorithms on neurofunctional data has been limited to more homogeneous data sets of dozens of participants. More recently, larger brain imaging data sets have allowed for the application of deep learning techniques to classify brain states and clinical groups solely from neurofunctional features. Deep learning techniques provide helpful tools for classification in healthcare applications, including classification of structural 3D brain images. Recent approaches improved classification performance of larger functional brain imaging data sets, but they fail to provide diagnostic insights about the underlying conditions or provide an explanation from the neural features that informed the classification. We address this challenge by leveraging a number of network visualization techniques to show that, using such techniques in convolutional neural network layers responsible for learning high-level features, we are able to provide meaningful images for expert-backed insights into the condition being classified. Our results show not only accurate classification of developmental dyslexia from the brain imaging alone, but also provide automatic visualizations of the features involved that match contemporary neuroscientific knowledge, indicating that the visual explanations do help in unveiling the neurological bases of the disorder being classified.

Keywords Visual Explanation · Deep Learning · Dyslexia · Neuroimaging · fMRI

L. Tomaz, D. D. Ruiz, F. Meneguzzi, N. B. Esper *, A. Buchweitz **
PUCRS, School of Technology, Porto Alegre 90619-900, Rio Grande do Sul, Brazil
*, **PUCRS, Graduate School of Medicine, Neurosciences, Porto Alegre 90619-900, Rio Grande do Sul, Brazil
*, **BraIns, Brain Institute of Rio Grande do Sul, Porto Alegre 90619-900, Rio Grande do Sul, Brazil
* PUCRS, School of Health and Life Sciences, Psychology, Porto Alegre 90619-900, Rio Grande do Sul, Brazil
E-mail: laura.tomaz@edu.pucrs.br, duncan.ruiz@pucrs.br, felipe.meneguzzi@pucrs.br, nathalia.esper@acad.pucrs.br, augusto.buchweitz@pucrs.br

1 Introduction

Brain imaging techniques such as structural MRI, functional MRI (fMRI) and diffusion-weighted imaging (DWI), can be used to find altered cortical tissue, structure and function associated with mental health disorders (Atluri et al., 2013). These techniques allow for the identification of neural markers, which in turn may provide or inform a diagnosis based on image features (Association et al., 2013).

Recent advances in deep learning have led researchers to employ machine learning to automate the analysis of medical imaging, including neurological images (Craddock et al., 2009; Tamboer et al., 2016; Froehlich et al., 2014). The most successful technique derived from deep learning for image classification consists of building neural network with convolutional layers, i.e. Convolutional Neural Networks (CNNs). The CNN specializes in processing multiple arrays, such as images (2D), audio and video or volumetric data (3D) (Bengio et al., 2015).

Brain imaging volumes have tens of thousands of voxels (3D-pixel) per image. Neurofunctional indices are mapped to these voxels, which makes feature selection a challenge for most machine learning approaches. Supervised approaches to machine learning relied on experts for feature selection (Bengio et al., 2015). Deep learning approaches obviate the dependence on supervision by automatically learning the features that better represent the problem domain (Bengio et al., 2015). Before deep learning methods were effectively applied to classification of brain imaging data, support vector machine (SVM) learning algorithms was the frequent choice for machine learning analyses of brain imaging (Cortes and Vapnik, 1995). SVM algorithms have the ability to generalize well in smaller fMRI datasets (Just et al., 2017; Li et al., 2014; Buchweitz et al., 2012; Murphy, 2012; Craddock et al., 2009; Tamboer et al., 2016; Froehlich et al., 2014), which are typically in the dozens of participants due to the high costs of fMRI scans (Craddock et al., 2009; Froehlich et al., 2014). Moreover, SVM models trained with linear kernels offer relatively straightforward explanations. This SVM property may be useful to break the “curse of dimensionality” by reducing the risk of overfitting the training data. The number of voxels used in feature selection should be reduced as much as possible.

Feature selection for brain imaging data is often performed on voxels in anatomically or functionally defined regions-of-interest (ROIs) based on the literature (Wolfers et al., 2015) or by data-driven methods that establish clusters of stable voxels (Just et al., 2014; Shinkareva et al., 2008). By contrast, deep learning models learn feature hierarchies at several levels of abstraction, which allows the system to learn complex functions independent of human-crafted features (Bengio et al., 2015). CNNs are applicable to a variety of medical image analysis problems, such as disorder classification (Heinsfeld et al., 2018), anatomy or tumor segmentation (Kamnitsas et al., 2017), lesion detection and classification (Ghafoorian et al., 2017), survival prediction (van der Burgh et al., 2017), and medical image construction (Li et al., 2014). Although these models can be accurate, their conclusions are opaque to human understanding and lack a straightforward explanation to help diagnosis. It is thus difficult for healthcare practitioners to apply and trust the results of machine learning models of brain imaging to assist them in their clinical diagnoses. Providing accurate visual representation of neural networks involved in deep learning classification may be a step in the direction of improving diagnostic application of classification using neurofunctional indices.

Groups	Typical Readers	Dyslexics
No. of Subjects	16	16
Age (mean \pm STD)	8.44 \pm 0.51	9.63 \pm 0.88
Sex (Male / Female)	09 / 07	11 / 05

Table 1: Demographic information of children included in the study.

The goal of the present study is to employ feature visualization techniques for CNNs. These techniques produce visual explanations of the key brain regions used to classify patients based solely on brain function. The key contribution is a visual representation of the regions involved in classifying whether children are dyslexic or not. The present technique provides a better understanding of CNN behavior and may provide practitioners with a tool to glean neural alterations associated with a disorder from functional brain imaging scans.

2 Method

2.1 Data

The brain imaging data was collected as part of a research initiative to investigate the neural underpinnings of dyslexic children in Brazil. The participants were diagnosed with dyslexia following a multidisciplinary evaluation that included medical history, reading and writing tests (Toazza et al., 2017; Costa et al., 2015), and an IQ test (Wechsler Abbreviated Scale of Intelligence (Wechsler, 2012)). The dyslexics readers were evaluated as part of an umbrella project that aims to establish a brain database of dyslexic readers of Brazilian Portuguese (Buchweitz et al., 2019; Costa et al., 2015). The typical readers were part of a longitudinal investigation of children learning to read (Buchweitz et al., 2019).

2.1.1 Participants

The present study included 32 children who were divided into two groups: typical readers (TYP; $n = 16$) and dyslexic readers (DYS; $n = 16$) (Buchweitz et al., 2019). The participants were all monolingual speakers of Portuguese and right-handed. The two groups were matched for age, sex and IQ [age 7–13 (9 ± 1.39)]. The typical readers children were evaluated at the end of the 2014 school year, and were scanned during the 2015 school year. The 16 dyslexic children were scanned between 2014 and 2015 (Buchweitz et al., 2019). Table 1 summarizes the complete demographics on this dataset.

2.1.2 Word-reading task

Task based fMRI examines brain regions whose activity changes from baseline in response to the performance of a task or stimulus (Petersen and Dubis, 2012). The study was designed as a mixed event-related experiment using a word and pseudoword reading test validated for Brazilian children (Salles et al., 2013). The task consisted of 20 regular words, 20 irregular words, and 20 pseudowords. The

60 stimuli were divided into two 30-item runs to give the participants a break halfway into the task. Words and pseudowords were presented on the screen one at a time for 7 seconds each. A question was presented to participants along with each word ("Does the word exist?"), to which participants had to select "Yes" or "No" by pressing response buttons. After 10 trials (10 words) either a baseline condition or rest period was inserted in the experimental paradigm. The baseline condition consisted of presentation of a plus sign "+" in the middle of the screen for 30 seconds, during which participants were instructed to relax and clear their minds.

2.1.3 Data acquisition

Data was collected on a GE HDxT 3.0 T MRI scanner with an 8-channel head coil (Buchweitz et al., 2019). The following MRI sequences were acquired: a T1 structural scan (TR/TE = 6.16/2.18 ms, isotropic 1mm^3 voxels); two task-related 5-min 26-sec functional fMRI EPI sequences; and a 7-min resting state sequence. The task and the resting-state EPI sequences used the following parameters: TR = 2000 ms, TE = 30 ms, 29 interleaved slices, slice thickness = 3.5 mm; slice gap = 0.1 mm; matrix size = 64×64 , FOV = 220×220 mm, voxel size = $3.44 \times 3.44 \times 3.60$ mm (Buchweitz et al., 2019).

2.1.4 Data preprocessing

The preprocessing steps for the task-based (word-reading task) fMRI are described as follows. Word-reading task: preprocessing included slice-time and motion correction, smoothing with a 6mm FWHM Gaussian kernel, and a nonlinear spatial normalization to $3.0 \times 3.0 \times 3.0$ mm voxel template (HaskinsPedsNL template). TRs with motion outliers (>0.9 mm) were censored from the data. The criteria for exclusion due to head motion were: excessive motion in 20% of the TRs. The average head motion for each group for the participants included in the study, in the word-reading paradigm, was: DYS M = 0.16 ± 0.08 , TYP M = 0.18 ± 0.15 . One participant from each group was excluded due to excessive head motion (Buchweitz et al., 2019).

2.2 Classification Task

We trained a number of deep learning models for the classification task using two key recent techniques in learning for image classification: CNNs (LeCun et al., 1998) and data augmentation (Perez and Wang, 2017). For the CNNs, we evaluated both two-dimensional (2D) and three-dimensional (3D) CNNs.

First, regarding the CNNs, our choice of model focuses on 2D CNNs due to the size of our dataset. Specifically, 2D CNNs have a smaller number of parameters in comparison to 3D CNNs (Szegedy et al., 2015). Thus, training a 3D CNN necessitates substantially larger datasets in order to generalize well. Indeed, our experiments show that 2D CNNs achieve superior accuracy to 3D CNNs given the limitations of our dataset. A 2D CNN takes an input having three dimensions (a height h , a width w , and a number of color channels or a depth d). This input volume is then processed by k filters, which operate on the entire volume of feature

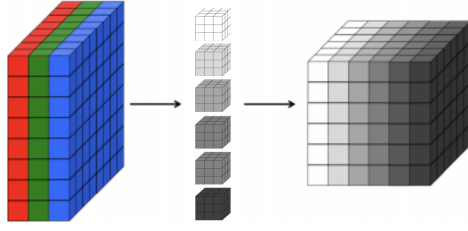


Fig. 1: A three-dimensional representation of a convolutional layer, each filter represents a slice in the output.

maps that have been generated at a particular layer. 2D convolutions have a pseudo third dimension comprising the color channels in each image, such that a 2D CNN applies convolutions to each channel separately, combining the resulting activations. Figure 1 illustrates each RGB channel in the input as a slice. A filter, which corresponds to weights in the convolutional layer, is then multiplied with a local portion of the input to produce a neuron in the next volumetric layer of neurons. In the Figure 1, the middle part represents filters, the depth of the filter corresponds to the depth of the input. The last cube in the figure represents the output activations of the combined convolution operations for each channel. The depth of the output volume of a convolutional layer is equivalent to the number of filters in that layer, that is, each filter produces its own slice. This can be viewed as using a 3D convolution for each output channel, which happens to have the same depth as the input (Buduma and Locascio, 2017). For this reason, it is possible to use volumetric images as inputs to a 2D CNN. In effect, this means that a 2D CNN processes the 3D volume of brain scan activations slice-by-slice.

Second, we avoid overfitting in our small dataset by employing data augmentation. Data augmentation is a technique (Perez and Wang, 2017) that provides the model with more data to increase the model’s ability to generalize from it. Such techniques are already employed in several image problems in deep learning models, but are still incipient in fMRI data (Mikołajczyk and Grochowski, 2018).

We adopted two approaches to build the 2D CNN architectures: i) use genetic programming, more specifically grammar-based genetic programming (GGP) fitted to our problem; and ii) employ a modified version of the LeNet-5 (LeCun et al., 1998) classification model. We then trained the resulting architecture using our dataset, and compared the effectiveness of 3D convolutions by converting the generated 2D CNNs into 3D ones by swapping the 2D convolutional layers to appropriately-sized 3D convolutions.

2.3 Visual Explanations Task

While many application areas for machine learning focus simply on model performance, recent work has highlighted the need for explanations for the decisions of trained models. Most users of machine learning often want to understand the trained models in order to gain confidence in the predictions. This is especially true for machine learning models used in medical applications, where the consequences of each decision must be carefully explained to patients and other stake-

holders (Yang et al., 2018; Jin et al., 2019). Besides the explainability aspect required of direct medical applications, our key motivation is to allow neuroimaging specialists to derive new insights on underpinnings of specific learning disorders such as dyslexia. Indeed, clinical diagnosis of dyslexia is reliable and costs less than using fMRI scans to validate such diagnostics (Torgesen, 1998; Ramus et al., 2003). However, researchers of dyslexia are interested in further understanding the disorder and its neural underpinnings *in-vivo* (Shaywitz et al., 2001; Hoeft et al., 2011). For this reason, building data-driven diagnostics models via machine learning and generating explanations for such models can be an invaluable tool for dyslexia research.

Recent research developed several methods for understanding and visualizing CNNs, in part as a response to criticism that the learned features in a neural network are not interpretable to humans (Zeiler and Fergus, 2013; Szegedy et al., 2013; Zhou et al., 2016). A category of techniques that aim to help understand which parts of an image a CNN model uses to infer class labels is called Class Activation Mapping (CAM) (Zhou et al., 2016). CAM produces heatmaps of class activations over input images. A class activation heatmap is a 2D grid of scores associated with a particular output class, computed for every location for an input image, indicating how important each location is with respect to that output class (Zhou et al., 2016). CAM can be used by a restricted class of image classification CNNs, precluding the model from containing any fully-connected layers and employing global average pooling (GAP).

A recent approach to visualize features learned by a CNN is GRAD-CAM (Selvaraju et al., 2017). GRAD-CAM is a generalization of CAM and can be applied to a broader range of CNN models without the need to change their architecture. Instead of trying to propagate back the gradients, GRAD-CAM infers a downsampled relevance heatmap of the input pixels from the activation heatmaps of the final convolutional layer. The downsampled heatmap is upsampled to obtain a coarse relevance heatmap. This approach has two key advantages: first, it can be applied to any CNN architecture; and second, it requires no re-training or change in the existing neural network architecture.

Figure 2 illustrates the GRAD-CAM approach. Given an image and a class of interest (in the example, ‘tiger cat’) as input, GRAD-CAM first forward propagates the image through the CNN part of the model and then through task-specific computations to obtain a raw score for the category. Next, GRAD-CAM sets all the gradients that do not belong to the desired class (tiger cat), which are originally set to one, are set to zero. GRAD-CAM then backpropagates this signal to the rectified convolutional feature maps of interest, which it combines to compute the coarse GRAD-CAM localization (the blue heatmap in the figure) which represents where the model has to look to make the particular decision. Finally, GRAD-CAM pointwise multiplies the heatmap with guided backpropagation to get Guided GRAD-CAM visualizations which are both high-resolution and concept-specific (Selvaraju et al., 2017).

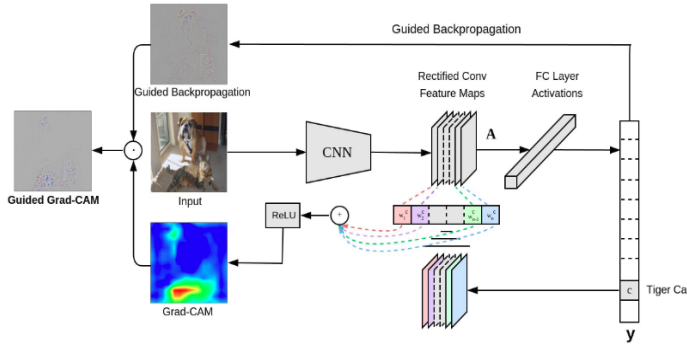


Fig. 2: GRAD-CAM overview (Selvaraju et al., 2017).

3 Experiments and Results

3.1 Classification

The deep learning classification model was implemented using the Keras open source library (Chollet et al., 2015) and trained with an Nvidia Geforce GTX 1080 Ti graphical processing unit (GPU) with 12 GB of memory. In our genetic programming (GP) approach, we generated a population of CNN architectures, such that each CNN architecture was an individual in a population, and which was evaluated to produce a fitness value. Network topology for all CNNs generated was based on a specific grammar for our problem and a set of different hyperparameters.

We introduced four key modifications in our version of the LeNet-5 architecture. First, we added batch normalization layers in the convolutional layers to improve convergence and generalization (Ioffe and Szegedy, 2015). Second, we used RELU activations in the convolutional layers instead of tanh. Third, we changed the average pooling to max pooling in the subsampling layers. Finally, we used a dropout rate of 0.5 in the fully connected layer. Figure 3 illustrates our modified version of LeNet-5. Our model architecture contains approximately 175k parameters, a small amount in comparison to deeper architectures, such as VGG-16 (Simonyan and Zisserman, 2014), which contains over 138 million parameters.

Our 3D CNN was developed based on our 2D CNN model. We made the changes necessary to adapt 2D convolutions, 2D pooling layers to a 3D model. In order to fit our data to a 3D CNN model, we expanded our data adding one channel for gray images resulting in a 4-dimensional array as input to the network. The resulting architecture has over 3 million parameters.

We compared our induced deep learning models with the (SVMs) (Cortes and Vapnik, 1995) technique, which has been used in a substantial number of previous neuroimaging studies (Tamboer et al., 2016; Froehlich et al., 2014). Specifically, this technique is popular for fMRI applications because datasets typically have many features (voxels), but only a relatively small set of subjects.

We trained all models to classify the participants between dyslexics and typical readers using the Adam optimizer. We improved the performance of our classifier

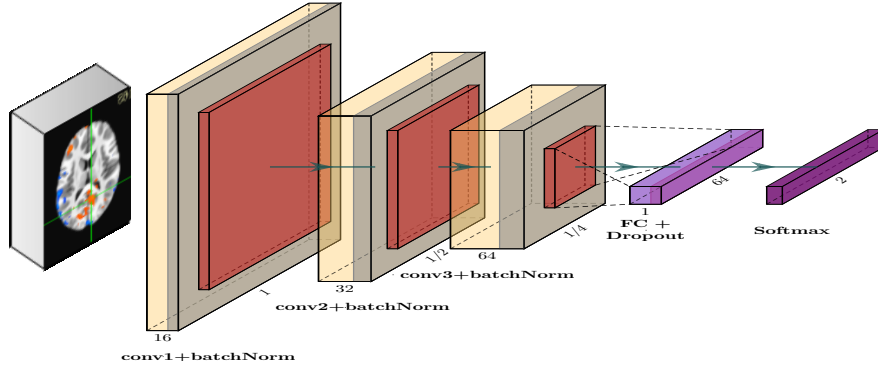


Fig. 3: Modified LeNet-5 overview

Hyperparameters	Values
Kernel size	Ranging from 1 to 5
# of filters	Starts with 16; duplicates after every convolution
Stride	Ranging from 1 to 3
Learning rate	Logarithmic range of [1, 0.1, 0.01, 0.001, 0.0001, 0.00001]
Dropout Rate	Tuned in the range of [0.1, 0.5, 1]
Batch size	16
# of epochs	Tuned in the range of [10, 50, 100]
# of Neurons FC layer	Tuned in the range of [32, 64, 128, 256, 512]

Table 2: CNN hyperparameters

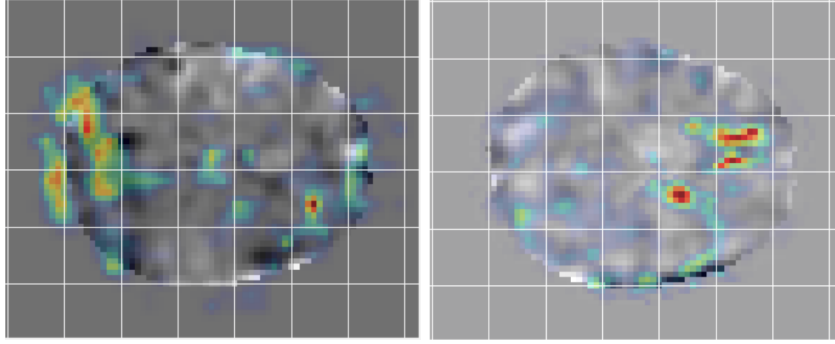
by employing two data augmentations to our dataset: i) we added Gaussian noise to fMRI images to generalize to noisy images; and ii) we added a random Gaussian offset, or contrast, to increase differences between images. The input of our machine and deep learning models was the whole brain volume ($60 \times 73 \times 60$ voxels) and a binary mask filling the brain volume to retrieve data from all brain regions. We split the dataset into train 80%, validation 10%, and test 10% sets. The parameter values including learning rate, dropout rate, batch size, and epoch size were optimized using the ranges summarized in Table 2. Note that we optimized the batch size to use the maximum available GPU memory.

All hyperparameters were optimized for both the 2D and 3D CNN models. For our SVM models, first, we applied an exhaustive search over specified parameters values for our SVM estimator. Second, we evaluated different methods of cross-validation. We report the results from splitting the data into train, validation, and test for Linear SVM implemented using scikit-learn (Pedregosa et al., 2011) library in Python.

Our modified version of LeNet-5 2D CNN network achieved 85.71% accuracy on subject classification. Our best GP 2D CNN model achieved an accuracy of 94.83% on subject classification. In comparison to the 2D CNN architecture, the 3D CNN, from both the modified LeNet-5 and GP approach, had an inferior accuracy on subject classification. The 3D CNN was also more prone to overfitting in the first few epochs of training. By contrast, the SVM approach achieved much lower

Technique	Accuracy
Best GP 2D CNN	94.83%
Modified LeNet-5	85.71%
Best GP 3D CNN	78.57%
Modified LeNet-5 3D	71.43%
SVM (80% train, 10% validation, 10% test)	70%

Table 3: Summary of Dyslexia Classification Results.



(a) Class activation mapping for dyslexic participants classification. (b) Class activation mapping for non-dyslexic participants classification.

Fig. 4: GRAD-CAM technique.

classification accuracy, regardless of the training dataset composition. Table 3 summarizes the results from all our classification approaches.

3.1.1 Visual Explanations

After training the 2D CNN model, we loaded the model with the best accuracy to visualize the learned gradients using GRAD-CAM technique (Selvaraju et al., 2017). The class activation generated by GRAD-CAM shows which regions were more instrumental to the classification.

To employ GRAD-CAM visualization to identify key differences between subjects and controls, we chose a pair of subjects as input, i.e. a control (non-dyslexic) subject and a dyslexic subject to generate the class activation mappings. Figures 4a and 4b show GRAD-CAM generated images of control and dyslexic subjects, with respect to the gradients learned by the network model. Both images depict the central slice from the axial view of the brain volume. Areas with lower class activation mappings are colored in gray, whereas areas with higher class activation mappings are color-coded from yellow (instrumental) to red (more instrumental). The color coding thus represents the brain regions impact on the model classification of subjects.

The visualization showed regions that were instrumental to the classification. The regions included: (i) the left occipital lobe (including left fusiform gyrus) with a high classification mapping for dyslexic participants; (ii) the anterior cingulate cortex (ACC) with a high classification mapping for typical readers (controls). Fig-

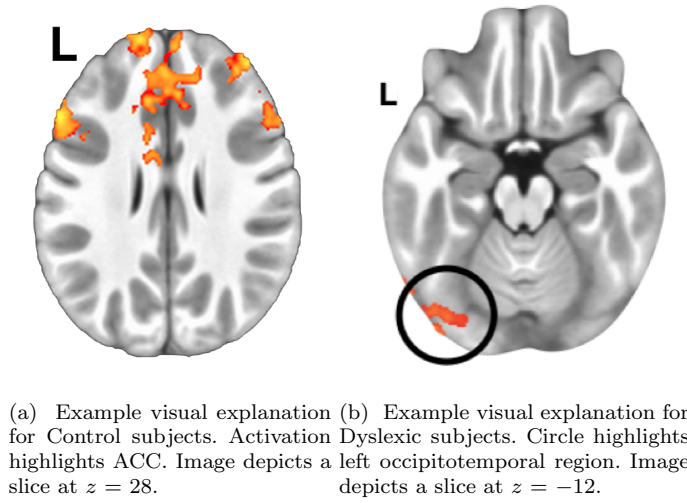


Fig. 5: AFNI (Cox, 1996) images showing brain activation from GRAD-CAM.

Figure 5b illustrates the classification mapping for dyslexia in left occipitotemporal region corroborates brain imaging findings that show functional alterations in this region associated with dyslexia and poor reading (Shaywitz et al., 2002; Martin et al., 2015). Figure 5a illustrates high classification mappings found in ACC for controls; activation of the ACC is usually associated with strategic control and attention processes (Chein and Schneider, 2005; Bush et al., 1999). More ACC activation has been found in association with additional attention processes engaged by early good readers, and in association with poor readers who benefited the most from reading remediation in (Shaywitz et al., 2002; Buchweitz et al., 2019; Shaywitz et al., 2003). Other regions with high classification mapping for dyslexia and controls are shown in Table 6.

4 Discussion and Related Work

To our knowledge, there is little work on visual explanations and brain imaging; for instance, a recent study used these explanations for Alzheimer’s disease (AD) and structural MRI (sMRI) (Jin et al., 2019). However, few approaches employed a visualization technique for MRI data, and there are none for fMRI data. The lack of approaches using brain imaging data of Dyslexia led us to search for related work employing deep learning to process any type of MRI data. Table 7 summarizes previous work that employed deep learning (Sarraf and Tofighi, 2016; Heinsfeld et al., 2018; Jin et al., 2019) for subject classification, and approaches that applied machine learning to identify participants with dyslexia (Cui et al., 2016; Tamboer et al., 2016; Płoński et al., 2017).

The machine learning techniques we use in this article allow us to divide the related work into two types: i) work that aimed to identify participants with dyslexia using traditional machine learning algorithms (e.g. SVM); and ii) work that used Deep Neural Networks (DNNs) in brain imaging data for disease classification,

Dyslexic		Regions	# voxels
Figure 6a	Left	Inferior Parietal	55
		Postcentral	72
		Precentral	9
		Precuneus	4
		Superior Parietal	24
		Supramarginal	26
Figure 6b	Left	Paracentral	2
		Postcentral	3
		Precentral	7
		Superior Frontal	12
	Right	Caudal Anterior Cingulate	18
		Inferior Parietal	73
		Paracentral	1
		Postcentral	63
		Precentral	49
		Precuneus	25
		Superior Frontal	10
		Superior Parietal	19
		Supramarginal	41
Figure 6c	Left	Superior Frontal	28
	Right	Superior Parietal	13
Figure 6d	Left	Caudal Anterior Cingulate	19
		Caudal Middle Frontal	40
		Posterior Cingulate	3
		Precentral	26
		Rostral Middle Frontal	21
		Superior Frontal	22
	Right	Caudal Anterior Cingulate	13
		Caudal Middle Frontal	53
		Posterior Cingulate	2
		Precentral	10
		Superior Frontal	49
		Superior Parietal	13

Table 4: Voxel count per brain region of Dyslexics for Figure 6. Brain Regions Instrumental for Dyslexic Identification with GRAD-CAM (Selvaraju et al., 2017). Region labels follow Haskins pediatric atlas (Molfese et al., 2015).

as follows. Sarraf and Tofghi (2016) employed the LeNet-5 architecture to classify patients with Alzheimer’s disease. Heinsfeld et al. (2018) used two stacked denoising autoencoders for the unsupervised pre-training stage to extract a lower-dimensional version of the ABIDE (Autism Brain Imaging Data Exchange) data. Jin et al. (2019) employed an attention-based 3D residual network based on the 3D ResNet to classify Alzheimer’s Disease classification and to identify important regions in their visual explanation task. The remaining work applied machine learning techniques to classify dyslexic and control subjects. Tamboer et al. (2016), and Cui et al. (2016) used SVM. Płoński et al. (2017) on top of using SVM, also used logistic regression (LR), and random forest (RF).

Approaches that adopt deep learning models (Sarraf and Tofghi, 2016; Heinsfeld et al., 2018; Jin et al., 2019) show that DNN approaches can achieve competitive results using MRI and fMRI data. Heinsfeld et al. (2018) achieved state-of-the-art results with 70% accuracy in identification of ASD versus control patients in the dataset. The authors that used classic machine learning techniques (Tamboer et al., 2016; Cui et al., 2016; Płoński et al., 2017) achieved 80%, 83.6%, and 65%

Typical Readers		Regions	# voxels
Figure 7a	Left	Caudal Middle Frontal	2
		Pars Opercularis	35
		Precentral	2
		Rostral Middle Frontal	12
	Right	Inferior Parietal	3
Figure 7b	Left	Caudal Anterior Cingulate	22
		Posterior Cingulate	1
		Precentral	7
		Rostral Middle Frontal	8
		Superior Frontal	59
	Right	Caudate	3
		Caudal Anterior Cingulate	6
		Superior Frontal	33
		Postcentral	63
		Superior Parietal	20

Table 5: Voxel count per brain region of Typical readers for Figure 7. Brain Regions Instrumental for Typical Readers Identification with GRAD-CAM (Selvaraju et al., 2017). Region labels follow Haskins pediatric atlas (Molfese et al., 2015).

		Regions	x	y	z
Dyslexic	Left	Fusiform Gyrus	-36	-75	-12
		Precuneus	-13	-54	16
		Cuneus	-10	-63	15
		Isthmus	-8	-55	16
		Pars Opercularis	-38	2	10
		Transversal	-41	-16	10
		Precentral	-53	2	10
	Right	Rostral	36	44	15
		Pars Triangularis	41	37	15
		Superior Frontal	3	64	15
		Insula	37	-3	11
Typical Readers	Left	Superior Frontal	0	41	28
		Caudate	-8	14	27
		Pars Opercularis	-50	20	28
	Right	Pars Opercularis	49	19	28
		Rostral	30	39	24

Table 6: Brain Regions Instrumental for Dyslexic and Typical Readers Identification with GRAD-CAM (Selvaraju et al., 2017). Region labels follow Haskins pediatric atlas (Molfese et al., 2015).

accuracy respectively on dyslexia prediction from anatomical scans. Performance of our deep learning models was consistent with other deep learning approaches for classification of neurological conditions. By contrast, our SVM results did not generalize as well as others (Cui et al., 2016; Tamboer et al., 2016; Płoński et al., 2017), but still outperformed another application of SVM for dyslexia classification (Płoński et al., 2017). Given the difference in datasets, we could not compare our approaches more directly.

Jin et al. (2019) visual explanations consisted of an attention map (much like a heatmap in visual representation) that indicated the significance of brain regions for AD classification. The authors compared their explanations to those generated by 3D-CAM and 3D-GRAD-CAM (Yang et al., 2018) methods. They (Jin et al.,

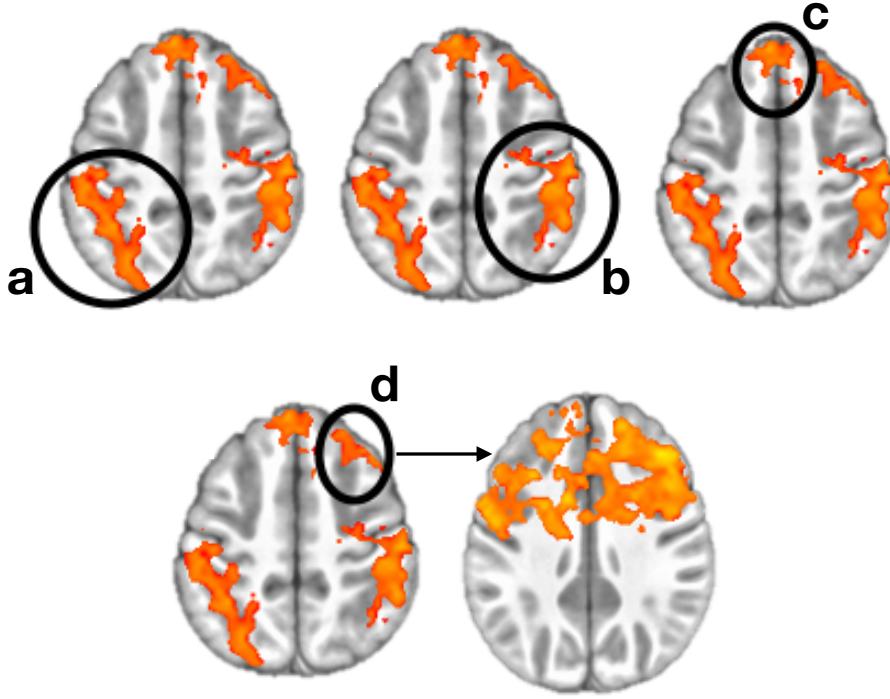


Fig. 6: Example visual explanation for Dyslexic subjects. Circle highlights instrumental brain regions for Dyslexic identification summarized in Table 4. The left side of the images represent the left side of the brain. Images *a, b, c, d* depict a slice at $z = 48$ and the last image depicts a slice at $z = 33$. AFNI (Cox, 1996) images showing brain activation from GRAD-CAM.

2019) observed that these two 3D methods led to a substantial drop in model performance when classifying subjects for Alzheimer’s Disease by the extra calculations needed to generate the heatmaps. By introducing the attention method, the authors obtained a 3D attention map for each testing sample and were able to identify the significance of brain regions related to changes in gray matter for AD classification. Our visualization technique may not be comparable to Jin et al. (2019), but the application of visualization techniques to medical imaging holds promise for making deep learning models interpretable.

5 Conclusion

We introduce a novel approach for the investigation of neural patterns in task-based fMRI that allow for the classification of dyslexic and control readers. While deep learning classifiers provide accurate identification of dyslexic versus control children based solely on their brain activation, such models are often hard to interpret. In this context, our main contribution is a visualization technique of the features that lead to specific classifications, which allows neuroscience domain

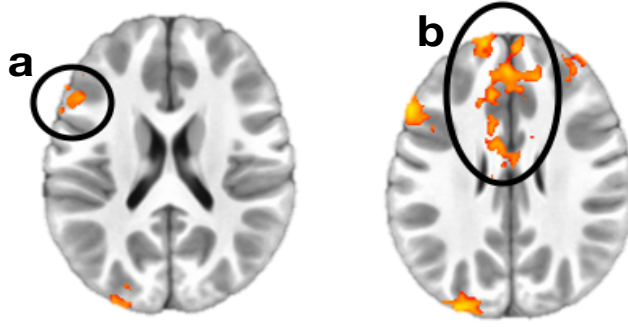


Fig. 7: Example visual explanation for Typical readers subjects. Circle highlights instrumental brain regions for Dyslexic identification summarized in Table 5. The left side of the images represent the left side of the brain. Image *a* depicts a slice at $z = 21$ and image *b* depicts a slice at $z = 27$. AFNI (Cox, 1996) images showing brain activation from GRAD-CAM.

experts to interpret the resulting models. Visual explanations of deep learning models allows us to compare regions instrumental to the classification with the latest neuroscientific evidence about dyslexia and the brain. The left occipital and inferior parietal regions that discriminated among groups are part of brain networks associated with phonological and lexical (word-level) processes in reading in different languages (Paulesu et al., 2001). Other regions reported in the visualization are also associated with reading and reading disorders. More activation of anterior right-hemisphere prefrontal regions (e.g. right pars triangularis) are associated with dyslexia and possible compensatory mechanisms (Vellutino et al., 2004; Shaywitz and Shaywitz, 2005).

Feature visualization techniques and visual explanations for deep learning models are a novel research area, and applying these techniques to neuroimaging data has the potential to help neuroscience research. Our work offers encouraging results, since the brain areas identified by the visual explanations are consistent with neuroscientific knowledge about the neural correlates of dyslexia. Nevertheless, there are a number of ways in which we can extend our work. The deep learning classification models can be applied to publicly available, large fMRI or MRI datasets to investigate the areas that are instrumental for identification of, for example, autism spectrum disorder. Moreover, other visualization techniques can be applied to provide a qualitative comparison among techniques when used to illustrate machine learning and deep learning studies of brain imaging.

References

- Association AP, et al. (2013) Diagnostic and statistical manual of mental disorders (DSM-5®). American Psychiatric Pub
- Atluri G, Padmanabhan K, Fang G, Steinbach M, Petrella JR, Lim K, MacDonald III A, Samatova NF, Doraiswamy PM, Kumar V (2013) Complex biomarker

Study Reference	Modality	Dataset	Classifier	Task	Accuracy
Proposed Method	Task based fMRI	ACERTA project	2D CNN	Subject classification for Dyslexia	94.83%
Sarraf and Tofghi (2016)	rs-fMRI	ADNI ³	LeNet-5	Subject classification for Alzheimer	96.86%
Jin et al. (2019)	sMRI	ADNI ³	Attention-based 3D ResNet	Subject classification for Alzheimer's Disease	92.1%
Cui et al. (2016)	sMRI	Private dataset	SVM	Subject classification for Dyslexia	83.6%
Tamboer et al. (2016)	sMRI	Non-disclosed dataset	SVM	Subject classification for Dyslexia	80%
Heinsfeld et al. (2018)	rs-fMRI	ABIDE	Denoising Autoencoder	Subject classification for Autism Spectrum Disorder	Above 70%
Płoński et al. (2017)	sMRI	Private dataset	SVM, LR, RF	Subject classification for Dyslexia	65%

¹ Dataset: <https://predict-hd.lab.uiowa.edu/>

² fcon_1000.projects.nitrc.org/indi/retro/cobre.htm

³ adni.loni.usc.edu

Table 7: Comparison with the classification scores of related work.

discovery in neuroimaging data: Finding a needle in a haystack. *NeuroImage: clinical* 3:123–131

- Bengio Y, Goodfellow IJ, Courville A (2015) Deep learning. *Nature* 521:436–444
- Buchweitz A, Shinkareva SV, Mason RA, Mitchell TM, Just MA (2012) Identifying bilingual semantic neural representations across languages. *Brain and Language* 120(3):282–289, DOI 10.1016/j.bandl.2011.09.003, URL <http://www.ncbi.nlm.nih.gov/pubmed/21978845><http://linkinghub.elsevier.com/retrieve/pii/S0093934X11001568>
- Buchweitz A, Costa AC, Toazza R, de Moraes AB, Cara VM, Esper NB, Aguzoli C, Gregolim B, Dresch LF, Soldatelli MD, et al. (2019) Decoupling of the occipitotemporal cortex and the brain's default-mode network in dyslexia and a role for the cingulate cortex in good readers: A brain imaging study of brazilian children. *Developmental neuropsychology* 44(1):146–157, DOI 10.1080/87565641.2017.1292516
- Buduma N, Locascio N (2017) Fundamentals of deep learning: Designing next-generation machine intelligence algorithms. " O'Reilly Media, Inc."
- van der Burgh HK, Schmidt R, Westeneng HJ, de Reus MA, van den Berg LH, van den Heuvel MP (2017) Deep learning predictions of survival based on mri in amyotrophic lateral sclerosis. *NeuroImage: Clinical* 13:361–369

- Bush G, Frazier JA, Rauch SL, Seidman LJ, Whalen PJ, Jenike MA, Rosen BR, Biederman J (1999) Anterior cingulate cortex dysfunction in attention-deficit/hyperactivity disorder revealed by fMRI and the counting stroop. *Biological Psychiatry* 45(12):1542–1552, DOI 10.1016/S0006-3223(99)00083-9, URL <http://www.sciencedirect.com/science/article/pii/S0006322399000839>
- Chein JM, Schneider W (2005) Neuroimaging studies of practice-related change: fMRI and meta-analytic evidence of a domain-general control network for learning. *Brain research Cognitive brain research* 25(3):607–23, DOI 10.1016/j.cogbrainres.2005.08.013, URL <http://www.ncbi.nlm.nih.gov/pubmed/16242923>
- Chollet F, et al. (2015) Keras. <https://keras.io>
- Cortes C, Vapnik V (1995) Support-vector networks. *Machine learning* 20(3):273–297
- Costa AC, Toazza R, Bassoa A, Portuguese MW, Buchweitz A (2015) Ambulatório de Aprendizagem do Projeto ACERTA (Avaliação de Crianças Em Risco de Transtorno de Aprendizagem): métodos e resultados em dois anos. In: Salles JF, Haase VG, Malloy-Diniz L (eds) *Neuropsicologia do Desenvolvimento: infância e adolescência*, Artmed, Porto Alegre, pp 151–158, URL <http://www.grupoa.com.br/livros/psicologia-cognitiva-comportamental-e-neurociencias/neuropsicologia-do-desenvolvimento/9788582712832>
- Cox RW (1996) AFNI: software for analysis and visualization of functional magnetic resonance neuroimages. *Computers and biomedical research, an international journal* 29(3):162–73, URL <http://www.ncbi.nlm.nih.gov/pubmed/8812068>
- Craddock RC, Holtzheimer III PE, Hu XP, Mayberg HS (2009) Disease state prediction from resting state functional connectivity. *Magnetic Resonance in Medicine: An Official Journal of the International Society for Magnetic Resonance in Medicine* 62(6):1619–1628
- Cui Z, Xia Z, Su M, Shu H, Gong G (2016) Disrupted white matter connectivity underlying developmental dyslexia: a machine learning approach. *Human brain mapping* 37(4):1443–1458
- Frøehlich C, Meneguzzi F, Franco A, Buchweitz A (2014) Classifying brain states for cognitive tasks: a functional mri study in children with reading impairments. In: *Proceedings of the XXIV Brazilian Congress on, Biomedical Engineering*, pp 2476–2479
- Ghafoorian M, Karssemeijer N, Heskes T, Bergkamp M, Wissink J, Obels J, Keizer K, de Leeuw FE, van Ginneken B, Marchiori E, et al. (2017) Deep multi-scale location-aware 3D convolutional neural networks for automated detection of lacunes of presumed vascular origin. *NeuroImage: Clinical* 14:391–399
- Heinsfeld AS, Franco AR, Craddock RC, Buchweitz A, Meneguzzi F (2018) Identification of autism spectrum disorder using deep learning and the abide dataset. *NeuroImage: Clinical* 17:16–23
- Hoelt F, McCandliss BD, Black JM, Gantman A, Zakerani N, Hulme C, Lyytinen H, Whitfield-Gabrieli S, Glover GH, Reiss AL, et al. (2011) Neural systems predicting long-term outcome in dyslexia. *Proceedings of the National Academy of Sciences* 108(1):361–366
- Ioffe S, Szegedy C (2015) Batch normalization: Accelerating deep network training by reducing internal covariate shift. *arXiv preprint arXiv:150203167*

- Jin D, Xu J, Zhao K, Hu F, Yang Z, Liu B, Jiang T, Liu Y (2019) Attention-based 3d convolutional network for alzheimer's disease diagnosis and biomarkers exploration. In: 2019 IEEE 16th International Symposium on Biomedical Imaging (ISBI 2019), IEEE, pp 1047–1051
- Just MA, Cherkassky VL, Buchweitz A, Keller TA, Mitchell TM (2014) Identifying autism from neural representations of social interactions: neurocognitive markers of autism. *PloS one* 9(12):e113879, DOI 10.1371/journal.pone.0113879
- Just MA, Pan L, Cherkassky VL, McMakin DL, Cha C, Nock MK, Brent D (2017) Machine learning of neural representations of suicide and emotion concepts identifies suicidal youth. *Nature human behaviour* 1(12):911, DOI 10.1038/s41562-017-0234-y
- Kamnitsas K, Ledig C, Newcombe VF, Simpson JP, Kane AD, Menon DK, Rueckert D, Glocker B (2017) Efficient multi-scale 3D cnn with fully connected crf for accurate brain lesion segmentation. *Medical image analysis* 36:61–78
- LeCun Y, Bottou L, Bengio Y, Haffner P, et al. (1998) Gradient-based learning applied to document recognition. *Proceedings of the IEEE* 86(11):2278–2324
- Li R, Zhang W, Suk HI, Wang L, Li J, Shen D, Ji S (2014) Deep learning based imaging data completion for improved brain disease diagnosis. In: Golland P, Hata N, Barillot C, Hornegger J, Howe R (eds) *Medical Image Computing and Computer-Assisted Intervention – MICCAI 2014*, Springer International Publishing, Cham, pp 305–312
- Martin A, Schurz M, Kronbichler M, Richlan F (2015) Reading in the brain of children and adults: a meta-analysis of 40 functional magnetic resonance imaging studies. *Human brain mapping* 36(5):1963–81, DOI 10.1002/hbm.22749, URL <http://www.ncbi.nlm.nih.gov/pubmed/25628041>
- Mikołajczyk A, Grochowski M (2018) Data augmentation for improving deep learning in image classification problem. In: 2018 International Interdisciplinary PhD Workshop (IIPHDW), pp 117–122, DOI 10.1109/IIPHDW.2018.8388338
- Molfese PJ, Glen D, Mesite L, Pugh KR, Cox RW (2015) The haskins pediatric brain atlas. *studies* 54:313–327
- Murphy KP (2012) *Machine learning: a probabilistic perspective*. MIT press
- Paulesu E, Démonet JF, Fazio F, McCrory E, Chanoine V, Brunswick N, Cappa SF, Cossu G, Habib M, Frith CD, et al. (2001) Dyslexia: Cultural diversity and biological unity. *Science* 291(5511):2165–2167, DOI 10.1126/science.1057179
- Pedregosa F, Varoquaux G, Gramfort A, Michel V, Thirion B, Grisel O, Blondel M, Prettenhofer P, Weiss R, Dubourg V, Vanderplas J, Passos A, Cournapeau D, Brucher M, Perrot M, Duchesnay E (2011) Scikit-learn: Machine learning in Python. *Journal of Machine Learning Research* 12:2825–2830
- Perez L, Wang J (2017) The effectiveness of data augmentation in image classification using deep learning. *arXiv preprint arXiv:171204621*
- Petersen SE, Dubis JW (2012) The mixed block/event-related design. *Neuroimage* 62(2):1177–1184
- Płoński P, Gradkowski W, Altarelli I, Monzalvo K, van Ermingen-Marbach M, Grande M, Heim S, Marchewka A, Bogorodzki P, Ramus F, et al. (2017) Multi-parameter machine learning approach to the neuroanatomical basis of developmental dyslexia. *Human brain mapping* 38(2):900–908
- Ramus F, Pidgeon E, Frith U (2003) The relationship between motor control and phonology in dyslexic children. *Journal of Child Psychology and Psychiatry* 44(5):712–722

- Salles JFd, Piccolo LdR, Zamo RdS, Toazza R (2013) Normas de desempenho em tarefa de leitura de palavras/pseudopalavras isoladas (lpi) para crianças de 1º ano a 7º ano. *Estudos e Pesquisas em Psicologia* 13(2):397–419
- Sarraf S, Tofighi G (2016) Classification of alzheimer’s disease using fmri data and deep learning convolutional neural networks. CoRR abs/1603.08631, URL <http://arxiv.org/abs/1603.08631>, 1603.08631
- Selvaraju RR, Cogswell M, Das A, Vedantam R, Parikh D, Batra D (2017) Grad-cam: Visual explanations from deep networks via gradient-based localization. In: *Proceedings of the IEEE International Conference on Computer Vision*, pp 618–626
- Shaywitz BA, Shaywitz SE, Pugh KR, Fulbright RK, Mencl WE, Constable RT, Skudlarski P, Fletcher JM, Lyon GR, Gore JC (2001) The neurobiology of dyslexia. *Clinical Neuroscience Research* 1(4):291–299
- Shaywitz BA, Shaywitz SE, Pugh KR, Mencl WE, Fulbright RK, Skudlarski P, Constable RT, Marchione KE, Fletcher JM, Lyon GR, et al. (2002) Disruption of posterior brain systems for reading in children with developmental dyslexia. *Biological psychiatry* 52(2):101–110
- Shaywitz SE, Shaywitz BA (2005) Dyslexia (specific reading disability). *Biological psychiatry* 57(11):1301–9, DOI 10.1016/j.biopsych.2005.01.043, URL <http://www.sciencedirect.com/science/article/pii/S0006322305001204>
- Shaywitz SE, Shaywitz BA, Fulbright RK, Skudlarski P, Mencl W, Constable R, Pugh KR, Holahan JM, Marchione KE, Fletcher JM, Lyon G, Gore JC (2003) Neural systems for compensation and persistence: young adult outcome of childhood reading disability. *Biological Psychiatry* 54(1):25–33, DOI 10.1016/S0006-3223(02)01836-X, URL <http://www.sciencedirect.com/science/article/pii/S000632230201836X>
- Shinkareva SV, Mason RA, Malave VL, Wang W, Mitchell TM, Just MA (2008) Using fmri brain activation to identify cognitive states associated with perception of tools and dwellings. *PLoS One* 3(1):e1394
- Simonyan K, Zisserman A (2014) Very deep convolutional networks for large-scale image recognition. arXiv preprint arXiv:14091556
- Szegedy C, Zaremba W, Sutskever I, Bruna J, Erhan D, Goodfellow I, Fergus R (2013) Intriguing properties of neural networks. arXiv preprint arXiv:13126199
- Szegedy C, Liu W, Jia Y, Sermanet P, Reed S, Anguelov D, Erhan D, Vanhoucke V, Rabinovich A (2015) Going deeper with convolutions. In: *Proceedings of the IEEE conference on computer vision and pattern recognition*, pp 1–9
- Tamboer P, Vorst H, Ghebreab S, Scholte H (2016) Machine learning and dyslexia: Classification of individual structural neuro-imaging scans of students with and without dyslexia. *NeuroImage: Clinical* 11:508–514
- Toazza R, Costa A, Bassôa A, Portuguese MW, Buchweitz A (2017) Avaliação de Dislexia do Desenvolvimento no Ambulatório de Aprendizagem do Projeto ACERTA. In: Navas A, Azoni CS, Oliveira DG, Borges JP, Mousinho R (eds) *Guia de boas práticas: do diagnóstico à intervenção de pessoas com transtornos específicos de aprendizagem*, Instituto ABCD, São Paulo, pp 26–33
- Torgesen J (1998) Catch them before they fall: Identification and assessment to prevent reading failure in young children (on-line). National Institute of Child Health and Human Development Available: ldonline.org/ld_in-depth/reading/torgesen.catchthem.html pp 1–15

- Vellutino FR, Fletcher JM, Snowling MJ, Scanlon DM (2004) Specific reading disability (dyslexia): What have we learned in the past four decades? *Journal of Child Psychology and Psychiatry and Allied Disciplines* 45(1):2–40, DOI 10.1046/j.0021-9630.2003.00305.x
- Wechsler D (2012) Wechsler preschool and primary scale of intelligence—fourth edition. The Psychological Corporation San Antonio, TX
- Wolfers T, Buitelaar JK, Beckmann CF, Franke B, Marquand AF (2015) From estimating activation locality to predicting disorder: a review of pattern recognition for neuroimaging-based psychiatric diagnostics. *Neuroscience & Biobehavioral Reviews* 57:328–349
- Yang C, Rangarajan A, Ranka S (2018) Visual explanations from deep 3d convolutional neural networks for alzheimer’s disease classification. In: *AMIA Annual Symposium Proceedings*, American Medical Informatics Association, vol 2018, p 1571
- Zeiler MD, Fergus R (2013) Visualizing and understanding convolutional networks. *CoRR* abs/1311.2901, URL <http://arxiv.org/abs/1311.2901>, 1311.2901
- Zhou B, Khosla A, Lapedriza A, Oliva A, Torralba A (2016) Learning deep features for discriminative localization. In: *Proceedings of the IEEE conference on computer vision and pattern recognition*, pp 2921–2929